Multimodal Graph Convolutional Network on Brain Structure and Function in Adolescent Anxiety and Depression

Sébastien Dam, Jean-Marie Batail, Pierre Maurel, Julie Coloigner

Multimodal Graph Convolutional Network on Brain Structure and Function in Adolescent Anxiety and Depression

Sébastien Dam, *Student Member, IEEE,* Jean-Marie Batail, Pierre Maurel, and Julie Coloigner

***Abstract*—Multimodal analysis of Magnetic Resonance Imaging (MRI) data enables leveraging complementary information across multiple imaging modalities that may be incomplete when using a single modality. For brain connectivity analysis, graph-based methods, such as graph signal processing, are effective for capturing topological characteristics of the brain structure while incorporating neural activity signals. However, for tasks like group classification, these methods often rely on traditional machine learning algorithms, which may not fully exploit the underlying graph topology. Recently, Graph Convolutional Networks (GCN) have emerged as a powerful tool in brain connectivity research, uncovering complex nonlinear relationships within the data. Here, we develop a multimodal GCN model to jointly model brain structure and function to classify anxiety and depression in adolescents using the Boston Adolescent Neuroimaging of Depression and Anxiety dataset. The graph's topology is initialized from structural connectivity derived from diffusion MRI, while functional connectivity is incorporated as node features to improve distinction between anxious, depressed patients and healthy controls. Interpretation of key brain regions contributing to classification is enabled through Gradient-weighted Class Activation Mapping, revealing the influence of the frontal and limbic lobes in the diagnosis of the conditions, which aligns with previous findings in the literature. By comparing classification results and the most discriminative features between multimodal and unimodal GCN-based approaches, we demonstrate that our framework improves accuracy in most classification tasks and reveals significant patterns of brain alterations associated with anxiety and depression.**

***Index Terms*—Anxiety, depression, functional MRI, structural connectivity, graph convolutional networks.**

I. Introduction

ANXIETY and depression in adolescents are mental health conditions that negatively affect the quality of life [1]. Our current knowledge of the biological mechanisms behind those diseases is still limited, resulting in clinical diagnosis primarily relying on symptomatic and behavioral assessments. However, anxious and depressed patients display a broad spectrum of heterogeneous symptoms, often leading to imprecise and delayed diagnoses. Therefore, identifying precise biomarkers for the detection of these conditions could offer better insights of the cerebral underpinnings behind them.

Brain connectivity has been extensively studied for investigating clinical biomarkers of psychiatric diseases, using the so-called brain connectomics [2]–[4]. Structural connectivity (SC) is derived from diffusion-weighted imaging (DWI), a neuroimaging technique that enables the visualization of the brain's white matter tracts by highlighting the direction and integrity of water diffusion along neural pathways. Using tractography [5], these diffusion patterns are analyzed to map the anatomical connections between different brain regions, providing a detailed view of the brain's structural network and connectivity patterns [6]. Functional connectivity (FC) captures the similarity between brain regions by measuring the correlation of blood oxygenation level dependent (BOLD) functional magnetic resonance imaging (fMRI) signals, acquired in the resting-state (rs-fMRI) [7]. Many neuroimaging studies have examined SC and FC to gain a deeper understanding of psychiatric disorders in adults [8], [9]. Among these, several papers have explored structural and functional brain connectomes of depression and reported disturbances in brain networks such as the default mode network (DMN), frontoparietal network (FPN) and cingulo-opercular network [10]–[12]. Similarly, a recent review and meta-analysis of rs-fMRI highlighted altered connectivity between the amygdala and prefrontal regions in patients with anxiety [13]. Investigating depression and anxiety in adolescents is equally important, as the onset of treatment-resistant conditions is often linked to the diagnosis of these disorders during adolescence [14]. However, there is still a lack of research focused on identifying biomarkers in adolescent populations. The main meta-analyses so far have found changes in FC in the DMN, the FPN, and the salience network [15], [16]. Although these findings are important, most studies have analyzed different modalities independently, which limits the overall understanding.

Integrating SC and FC allows for a more comprehensive analysis of brain networks by capturing complementary information measured by fMRI and DWI [17]–[19], particularly when characterizing psychiatric disorders such as autism, schizophrenia, and major depression [20], [21]. Several fusion (concurrent analysis of modalities) and integration (use of one modality to constrain another one) techniques have been implemented to combine multiple modalities in psychiatric research [22]. These methods include linked independent component analysis, which identifies modes of variations across modalities and disentangles independent sources of

Sébastien Dam, Pierre Maurel, and Julie Coloigner are with Univ Rennes, Inria, CNRS, Inserm, IRISA UMR 6074, Empenn ERL U 1228, F-35000 Rennes, France (e-mail: sebastien.dam@inria.fr; pierre.maurel@irisa.fr; julie.coloigner@irisa.fr).

Jean-Marie Batail is with Centre Hospitalier Guillaume Régnier, Pôle Hospitalo-Universitaire de Psychiatrie Adulte, Rennes, France, Centre Hospitalier Universitaire de Rennes, Institut National de la Santé et de la Recherche Médicale (INSERM), Rennes, France, and Faculté de Médecine, Rennes Université, Rennes, France (e-mail: jm.batail@ch-guillaumeregnier.fr).

variation. For instance, it has been used to fuse measures of cortical macrostructure, white matter diffusion properties and rs-fMRI DMN amplitude to study depression [23]. Similarly, multimodal independent vector analysis has been developed to estimate linked independent sources across multiple modalities [24]. Then, the outputs from these techniques are often used as features in machine learning models. In [23], for example, the authors submitted subject weights derived from linked independent component analysis to classify depressed patients and controls. However, these approaches not only rely on linear models, which may not be fully adequate when dealing with multimodal data where complexity arises from the interaction between different modalities, but they also overlook the valuable information embedded in the topological properties of brain connectivity.

Recently, graph structures have emerged as a promising way to bridge the gap between brain structure and function. Frameworks like Graph Signal Processing (GSP) attempt to project brain functional data onto its structural network, offering a more holistic view of brain organization [25]. Several studies leveraged GSP to analyze the coupling strengths between rs-fMRI time-series and SC for the classification of patients with disorders such as depression [26], anxiety [27], and Alzheimer's disease [28]. However, the common approach is to unroll graph-based measures extracted from each brain region into a vector and then to apply a wide range of multivariate classifiers, such as support vectors machines or random forests. Although these works achieved significant success, those machine learning approaches do not incorporate the graph topology and geometrical properties of the connectome. This limitation has spurred interest in researchers using deep learning approaches, specifically graph-based ones, which may be better suited for capturing the complex relationships between brain regions.

Kipf and Welling [29] demonstrated the power of Graph Convolutional Networks (GCN) to extend the convolutional operations from regular Euclidean data to graph-structured data and allowed the emergence of multiple applications of GCN in neuroimaging and brain connectivity [30], [31]. By leveraging the brain's structural or functional connectome as a graph, GCN exploit its topology to convey information between brain regions, making them an effective tool for understanding disruptions in brain networks associated with disorders. For example, Ktena et al. [32] proposed a siamese GCN, and employed spectral graph convolutions on brain imaging data to classify autism spectrum disorder based on fMRI data. The association of deep reinforcement learning with GCN was adopted in [33] to learn an optimal graph neural network (GNN) architecture, which was applied on multiple datasets covering different neurological disorders, including human immunodeficiency virus infection, bipolar disorder, or attention deficit hyperactivity disorder. To predict mild cognitive impairment, Zhang et al. [34] designed a cascaded deep model that integrated temporal features from functional activity using a recurrent neural network, alongside the brain structural connectome as the graph topology of the GCN, effectively fusing fMRI and diffusion tensor imaging data.

Based on these promising works, we propose a supervised framework for classification tasks. The main objective is to integrate FC with structural brain connectome and to identify sub-networks with significantly connectivity differences in binary classification. We hypothesize that a multimodal GCN-based approach jointly modeling SC and FC will be able to extract complementary information from both modalities, and thus allow enhanced classification performance and identification of salient regions of interest (ROI). Thanks to the GCN's ability to capture higher-order information from the neighborhoods of graph nodes representing ROIs in the SC, and incorporate neural activity features from FC, we believe that such a model will provide meaningful perspectives for multimodal analysis.

The main contributions of this paper can be summarized as follows:

- We develop a multimodal GCN-based model for classification tasks using SC and FC. Moreover, we adapt the Gradient-weighted Class Activation Method (Grad-CAM) [35] to our model in order to identify the sub-networks exhibiting the most discriminant features among two groups.
- We hypothesize that multimodal methods outperform unimodal ones. To verify that, we test our model against methods which take as input only a single modality, such that structural or functional data are exclusively used.
- We train and test our model on clinical data for graph classification, and design experiments on anxious and depressed adolescent from the Boston Adolescent Neuroimaging of Anxiety and Depression (BANDA) open dataset [36].

The remainder of the paper is structured as follows. First, we present our multimodal multi-layer GCN model for our study in Section II. Then, we describe our experiments in Section III. We expose our classification performance and the salient brain regions subsequently obtained in Section IV, which are followed by their interpretation in a discussion in Section V. Finally, we conclude the paper in Section VI.

II. Methods

In this section, we introduce our multimodal GCN framework for the classification of anxiety and depressed patients. First, in Section II-A, we briefly present some key concepts from GSP. Second, in Section II-B, extension of graph convolution from GSP to our setting is presented. Then, Section II-C is devoted to our multimodal GCN model for jointly modeling FC and the underlying brain structure. Finally, in order to interpret the salient features obtained from the trained model, we extended the Grad-CAM technique to our graph setting in Section II-D.

A. Graph Signal Processing

Let $\mathcal{G} = \mathcal{G}(\mathcal{V}, \mathcal{E}, \boldsymbol{A})$ be an undirected graph with N nodes, where $\mathcal{V}$ is the set of nodes with each node representing a distinct ROI and $\mathcal{E}$ is the set of undirected edges in $\mathcal{G}$. The matrix $\boldsymbol{A}$ is a symmetric weighted matrix representing the adjacency matrix where each entry is the strength of connection

between two ROIs. The graph normalized Laplacian matrix is defined as

$$\boldsymbol{L} = \boldsymbol{I}_N - \boldsymbol{D}^{-1/2}\boldsymbol{A}\boldsymbol{D}^{-1/2}, \tag{1}$$

where $\boldsymbol{D}$ is the diagonal matrix of node degrees, i.e., $d_{ii} = \sum_j a_{ij}$. Since it is real, symmetric, and positive semi-definite, it can be diagonalized via its eigendecomposition as $\boldsymbol{L} = \boldsymbol{U}\boldsymbol{\Lambda}\boldsymbol{U}^\top$, where the columns of $\boldsymbol{U} = [\boldsymbol{u}_1, \boldsymbol{u}_2, \ldots, \boldsymbol{u}_N]$ are the orthonormal eigenvectors, and $\boldsymbol{\Lambda}$ is the diagonal matrix that stores the non-negative eigenvalues $\boldsymbol{\Lambda} = \mathrm{diag}(\lambda_1, \lambda_2, \ldots, \lambda_N)$. The k^{th} eigenvalue λ_k reflects a notion of frequency of the corresponding eigenvector $\boldsymbol{u}_k$, which can be interpreted as a structural harmonic.

Let $\boldsymbol{x} \in \mathbb{R}^N$ be a graph signal, where x_n denotes the signal value at node n. The signal $\boldsymbol{x}$ can then be projected on the structural harmonics through the graph Fourier transform (GFT) to perform a frequency analysis of the graph signal, as defined as

$$\hat{\boldsymbol{x}} = \boldsymbol{U}^\top \boldsymbol{x}. \tag{2}$$

B. Graph Convolutional Networks

Here, we introduce spectral graph convolution, which serves as a fundamental operation in GCN. The latest extends traditional convolutional techniques to graph-structured data, allowing the aggregation of information from neighboring nodes to learn efficient node representations for classification tasks. Given a graph signal $\boldsymbol{x}$ and a filter $\boldsymbol{\Theta}$, graph convolution can be defined as

$$\boldsymbol{\Theta} * \boldsymbol{x} = \sum_{k=0}^{K} \theta_k \boldsymbol{L}^k \boldsymbol{x}, \tag{3}$$

where $\boldsymbol{\Theta} = \sum_{k=0}^{K} \theta_k \boldsymbol{L}^k$ is a graph filter with coefficients $\boldsymbol{\theta} = [\theta_0, \ldots, \theta_K]$. The graph convolution operation aggregates signal values from K-hop neighborhoods in the graph. Filters designed this way are thus exactly localized, ensuring that the convolution only influences nodes within a fixed range. Based on the GFT, the filtered signal in (3) can be shifted in the spectral domain to perform spectral graph convolution, such that

$$\begin{aligned} \boldsymbol{U}^T \boldsymbol{\Theta} \boldsymbol{x} &= \boldsymbol{U}^T \sum_{k=0}^{K} \theta_k (\boldsymbol{L})^k \boldsymbol{x} = \boldsymbol{U}^T \sum_{k=0}^{K} \theta_k (\boldsymbol{U}\boldsymbol{\Lambda}\boldsymbol{U}^T)^k \boldsymbol{x} \\ &= \left(\sum_{k=0}^{K} \theta_k \boldsymbol{\Lambda}^k \right) \hat{\boldsymbol{x}}. \end{aligned} \tag{4}$$

For each frequency λ_i, the convolution is transformed into an element-wise multiplication between the filter's frequency response $\tilde{\theta}_i = \sum_{k=0}^{K} \theta_k \lambda_i^k$ and the signal's GFT coefficient $\hat{x}_i$.

To be able to define the filter $\tilde{\boldsymbol{\theta}}$ directly in the spectral domain, the eigendecomposition of $\boldsymbol{L}$ is required. However, its computational complexity can heavily impair the feasibility for large graphs. To circumvent this limitation, ChebNet [37] was proposed by introducing a filter defined by Chebyshev polynomials of the diagonal matrix of eigenvalues, i.e. $\boldsymbol{\Lambda}$, instead of conventional polynomials as in 4. A first-order polynomial graph convolution filter, which is used to define the so-called GCN model, has been proposed in [29] by assigning $K = 1$ and $\theta = \theta_0/2 = -\theta_1$, so that (3) simplifies to

$$\boldsymbol{\Theta} * \boldsymbol{x} = \theta \left(\boldsymbol{I}_N + \boldsymbol{D}^{-1/2}\boldsymbol{A}\boldsymbol{D}^{-1/2} \right) \boldsymbol{x}. \tag{5}$$

A graph convolutional network can be built by stacking layers of learnable graph convolutional filters of this form. This further leads to the formulation of the GCN layer as:

$$\boldsymbol{H}^{(l)} = \sigma \left(\tilde{\boldsymbol{A}} \boldsymbol{H}^{(l-1)} \boldsymbol{\Theta}^{(l)} \right), \tag{6}$$

where σ is the nonlinear activation function, $\boldsymbol{H}^{(l)}$ is the learned representations at layer l, $\boldsymbol{\Theta}^{(l)} \in \mathbb{R}^{F_i \times F_o}$ contains the learnable filter parameters, where F_i and F_o are the feature sizes of input and output graph signals, respectively, and are subject to the choice of the number of node features in the GCN layers. We propose to use $\tilde{\boldsymbol{A}} = \hat{\boldsymbol{D}}^{-1/2}\hat{\boldsymbol{A}}\hat{\boldsymbol{D}}^{-1/2}$, as in [29], which is the normalized adjacency matrix following the renormalization trick, where $\hat{\boldsymbol{A}} = \boldsymbol{A} + \boldsymbol{I}_N$ and $\hat{\boldsymbol{D}}_{ii} = \sum_j \hat{\boldsymbol{A}}_{ij}$. This has been shown to reduce some instability in training of GCN [29]. By stacking multiple GCN layers, information from distant neighbors can be transmitted across the graph. Fig. 1 depicts the principle of node features aggregation at different layers in a multi-layer GCN.

C. Multimodal GCN based patient classification

In this paper, we perform a multimodal GCN-based supervised framework, whose architecture is summarized in Fig. 2, for classification tasks. The model is trained on a cohort including two groups to capture population patterns in the SC-FC relationship while also reflecting subject-specific variability to discriminate among classes. The input graphs for the multimodal GCN model are individual subject-level brain graphs corresponding to the SC networks, which are represented by the symmetric adjacency matrix $\boldsymbol{A} \in \mathbb{R}^{N \times N}$. A graph signal matrix $\boldsymbol{X} \in \mathbb{R}^{N \times D}$ from the FC can also be input into the model as node attributes or graph signal associated to each node n, where each graph signal is now a vector of dimension D.

More explicitly, the multimodal GCN model consists of three hidden layers, each parameterized with 64 filters, defined in this work as:

$$\boldsymbol{H}^{(l)} = \begin{cases} \sigma \left(\tilde{\boldsymbol{A}} \boldsymbol{H}^{(l-1)} \boldsymbol{\Theta}^{(l)} \right), l \geq 1, \\ \boldsymbol{X}, l = 0, \end{cases} \tag{7}$$

ReLu is chosen as the nonlinear activation function. Subsequently, to obtain the entire representation of the graph or *graph-level embedding* $\bar{\boldsymbol{H}}$, the output from the third layer is fed into a global average pooling layer to reduce dimensionality and aggregate node information

$$\bar{\boldsymbol{H}} = \frac{1}{N} \sum_{i=1}^{N} \boldsymbol{H}_i^{(3)}. \tag{8}$$

Finally, the obtained graph-level embeddings are input into a dense layer for patient classification, and the final prediction z is expressed as

$$z = \mathrm{softmax}(\mathrm{dense}(\bar{\boldsymbol{H}})), \tag{9}$$

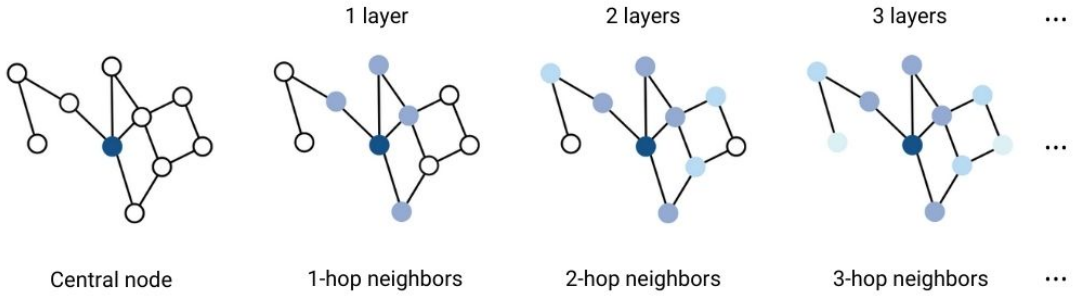

Fig. 1. GCN layers propagate node information by aggregating features over an increasing number of hops. Starting from a central node (dark blue), each additional layer expands the neighborhood by 1 hop, resulting in filters that are localized within k-hop supports. Nodes with the same color indicate those that are equidistant from the central node in terms of the shortest path. As more GCN layers are stacked, information from more distant nodes is incorporated, represented by the fading colors.

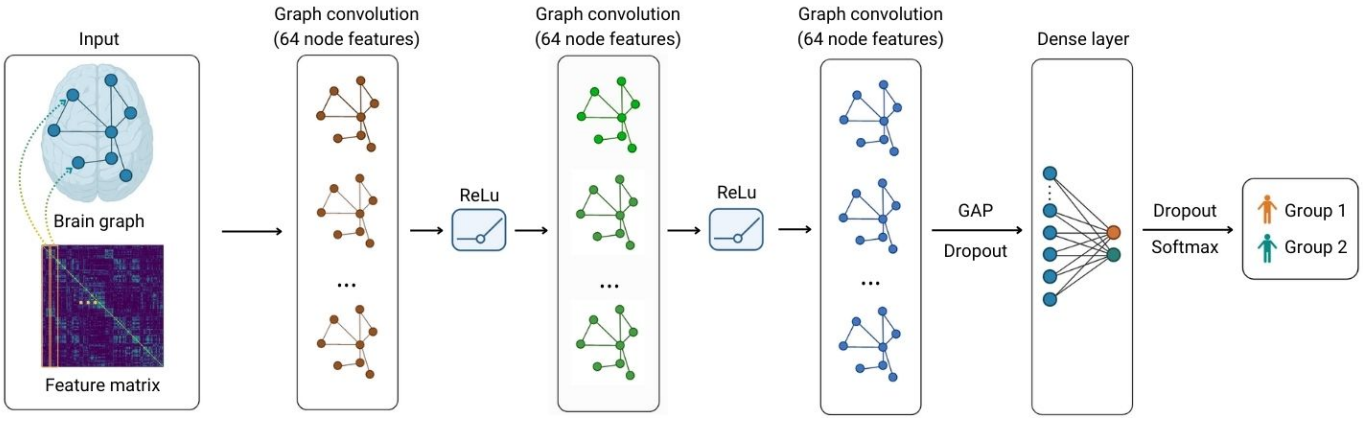

Fig. 2. The multimodal multi-layer GCN architecture. Based on the input brain graph represented by its weighted adjacency matrix, and the feature matrix, a GCN layer generates a hidden representation for each node by aggregating features from its neighboring nodes based on the neurons' weights. Following this aggregation, a nonlinear activation function is applied to the resulting hidden representation. By stacking multiple GCN layers, information from distant nodes are transmitted across the graph, until generating the final hidden representation, before being fed to a global average pooling layer and a dense layer. Finally, a softmax is applied to output the predictive probability of the input classes. GAP: global average pooling.

where softmax$(.)$ is used to normalize the raw output scores of the dense layer into the predictive probability of the input classes. For training, the cross-entropy loss is used as the loss function, which is computed as

$$\text{CE} = -\frac{1}{M}\sum_{i}\sum_{c=1}^{Z} y_{ic}\log(z_{ic}), \tag{10}$$

where M is the number of patients/graphs in the training set, C is the number of patient classes, $y_{ic} = 1$ if the label of patient i is equal to c, $y_{ic} = 0$ otherwise, and z_{ic} is the predicted probability of patient i in class c.

D. Interpretability of GCN

With the growing use of deep learning, several explanation methods have been proposed to interpret deep learning-based models predictions, such as Gradient-weighted Class Activation Mapping (Grad-CAM) [35]. Here, we adapt Grad-CAM to our setting to interpret our multimodal GCN model predictions and identify the ROIs that contribute the most to the discrimination of the classes. This approach was originally introduced to provide a localization map as a visualization explanation for convolutional neural networks models for tasks such as image classification, image captioning, or visual question answering [38], [39]. It essentially exploits the last convolutional layer and uses the gradient information flowing into it during the training step to assign importance values for each node. Let $\boldsymbol{H}_k^{(l)} \in \mathbb{R}^N$ be the k^{th} graph convolutional feature map at layer l:

$$\boldsymbol{H}_k^{(l)} = \sigma\left(\tilde{\boldsymbol{A}}\boldsymbol{H}^{(l-1)}\boldsymbol{\Theta}_k^{(l)}\right), \tag{11}$$

where $\boldsymbol{\Theta}_k^{(l)}$ is the k^{th} column of learnable matrix $\boldsymbol{\Theta}^{(l)}$. For each node n, we can denote $H_{k,n}^{(l)}$ as the k^{th} feature at layer l. Note that $\boldsymbol{H}_k^{(\Gamma)}$ represents the feature map of the final graph convolution layer. For each group c, the score (before softmax) can then be calculated as

$$s^c = \frac{1}{N}\sum_{k} w_k^c \sum_{n=1}^{N} H_{k,n}^{(\Gamma)}, \tag{12}$$

where w_k^c is the weight of the k^{th} feature map of the final layer for predicting group c. To obtain a map containing the most discriminative features, we compute the gradients of s^c, with respect to the k^{th} feature map after the final convolutional layer, *i.e.* $\frac{\partial s^c}{\partial H_{k,n}^{(\Gamma)}}$. These gradients flowing back are averaged

over the N nodes so as to obtain the Grad-CAM importance weights α_k^c:

$$\alpha_k^c = \frac{1}{N}\sum_{n=1}^{N}\frac{\partial s^c}{\partial H_{k,n}^{(\Gamma)}}. \quad (13)$$

Finally, the localization map G_n^c at the final GCN layer is retrieved by performing a weighted combination of forward feature maps, and followed by a ReLu in order to obtain the ROIs that have a positive contribution on the classification:

$$G_n^c = ReLu(\sum_k \alpha_k^c H_{k,n}^{(\Gamma)}). \quad (14)$$

Grad-CAM was performed on each individual. Subsequently, we computed the Euclidean mean activation value across all the individuals to reflect the contribution of each ROI in the brain connectivity graph.

III. Experiments

Data, preprocessing steps and experimental setting are described in this section.

A. Data

The BANDA study is one of the projects funded by the National Institute of Health to study a disease population using Human Connectome Project protocols [36]. This cohort includes 207 adolescents between 14 and 17 years old, with brain imaging data (62 Control (CA), 80 Anxious (AA) and 65 Depressed Adolescents (DA)). We discarded 15 subjects due to poor image quality, resulting in 192 subjects including 60 CA, 72 AA and 60 DA. Three modalities of brain imaging data (T1-weighted MRI, rs-fMRI and DWI) were acquired for each participant.

The T1-weighted MRI data was acquired with a field of view (FoV) of $256 \times 240 \times 167$ mm, 0.8 mm isotropic voxel size and TR $= 2400$ ms. The DWI images have 183 gradient directions, sampled on 2 shells of $b = 1500$ s/mm^2 and 3000 s/mm^2, an FoV of $210 \times 210 \times 138$ mm, 1.5 isotropic voxel size, TR $= 3230$ ms and TE $= 89.20$ ms. The rs-fMRI data has 420 volumes, acquired with an FoV of $208 \times 208 \times 144$ mm, 2.0 mm isotropic voxel size, TR $= 800$ ms, TE $= 37$ ms and flip angle $= 52°$.

B. Preprocessing

We preprocessed the data using QSIPrep [40] and fMRIPrep [41]. The anatomical preprocessing workflows contain intensity non-uniformity correction of the T1w image, skull-stripping, and brain tissue segmentation of cerebrospinal fluid, white-matter and gray-matter.

The DWI images were denoised using MP-PCA [42], then corrected for Gibbs unringing using local subvoxel-shifts, B1 field inhomogeneity using ANT's N4 algorithm, head motion and Eddy current using FSL's eddy [43]. Finally, the whole-brain cortical and subcortical Tian-Schaefer atlas [44], [45] with 400 cortical regions and 16 subcortical regions was adopted to construct SC matrices. Whole-brain probabilistic tractography including 10 million fibers was performed, using a spherical deconvolution approach and the Spherical-deconvolution Informed Filtering of Tractograms (SIFT2) [46]. The entries with less than 10 fibers were removed for each subject in an attempt to remove false-positive fibers.

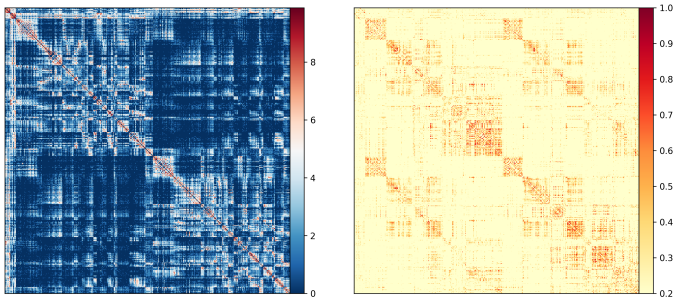

Fig. 3. Structural (left) and functional (right) connectivity matrices of a sample subject. The entries of the structural connectivity correspond to the number of fibers between two ROIs, and were log-transformed for visualization purposes, while those of the functional connectivity were obtained by computing the Pearson correlation coefficient of every pair of averaged BOLD signals.

For fMRI images, head-motion parameters (transformation matrices and six corresponding rotation and translation parameters) were estimated using FSL's mcflirt. A fieldmap was estimated based on two echo-planar imaging references with opposing phase-encoding directions, with FSL's topup. BOLD runs were also slice-time corrected using 3dTshift from AFNI. The same brain atlas was adopted and regional mean time-series were estimated by averaging the fMRI time-series over all voxels within each ROI. We decided to calculate the Pearson correlation coefficient of every pair of averaged BOLD signals as $\boldsymbol{P} \in \mathbb{R}^{N\times N}$, which serves as the feature matrix in (7). Each feature vector $\boldsymbol{p}_n = (p_{n1}, p_{n2}, ..., p_{nN})$ is thus the concatenation of correlations of node n to all the other nodes. This choice for the feature matrix is also termed *connection profile*, where each row in the Pearson matrix is used as the node features, has often been made in other works [47]. Similarly to SC matrices, we thresholded the correlations so as to keep the ones greater than 0.2 in order to remove spurious and weak correlations.

The SC and FC matrices of one subject are depicted in Fig. 3. The atlas was arranged such that the first ROIs correspond to the subcortical regions, followed by the cortical regions of the left and right hemispheres. Across the subjects, we note that the anatomical connections are predominantly within the same hemisphere, with fewer links across the left and right ones in SC. Moreover, subcortical regions present a high number of connections with all the brain regions, while cortical ones are connected to fewer ones. In contrast, FC shows more scattered correlations between hemispheres, suggesting that functional links exist between ROIs even in the absence of anatomical links. This observation motivates further exploration of the complementarity between these two modalities.

C. Experimental setting

To further investigate this complementarity, we implemented a multimodal GCN-based approach to assess how well it can

leverage both SC and FC patterns for classification.

Implementation details. All the experiments were run via 10-fold cross validation such that the data was randomly partitioned into 80% training, 10% validation and 10% test set. To avoid class imbalance during the data splitting, we carefully grouped the subjects in the sets so that they contain approximately the same percentage of samples of each class in each fold, using the stratified group k-fold technique. During the training process, the parameters were initialized following the Xavier scheme [48]. The models were trained for 250 epochs using the Adam optimizer with standard learning rate 0.001, $\beta_1 = 0.9$, $\beta_2 = 0.999$. The dropout rate was 0.3. Batch normalization was also applied after each GCN layer, with early stopping as well with a patience of 20 epochs. The models were trained on a Linux machine with 32 GB of RAM, and were implemented by using PyTorch Geometric extension library based on PyTorch 2.3 (Python 3.10) [49].

Comparative tests. A major objective of this study was to investigate whether integrating multimodal data in GCN enhanced classification performance compared to relying on unimodal data alone. To this end, we evaluated our multimodal GCN model with two input configurations that serve as comparative tests: the first used only DWI data and the second only fMRI, which we named *unimodal SC* and *unimodal FC*, respectively. For unimodal SC, for each participant, the graph input was the weighted adjacency matrix containing the number of fibers from tractography performed with the DWI data, and the node features were computed using the connection profile. For unimodal FC, for each participant, the graph input was the thresholded Pearson matrix $\boldsymbol{P}$ computed from the BOLD signals from fMRI data, and the node features were also computed using the connection profile. The training process remained unchanged, resulting in the learned representations capturing exclusively information related to either SC or FC only. Grad-CAM was applied to these models as well to compare the salient ROIs that were output when considering a unique modality. Fig. 4 illustrates our experimental pipeline.

Evaluation metrics. In this study, we used common metrics to assess the performance of our proposed multimodal model and the comparative tests, including Accuracy, F1-score, and Precision.

IV. Results

A. Classification performance

We tested 3 different classification tasks including CA vs AA, CA vs DA, and AA vs DA to examine the performance of our approach. For each task, we compared the evaluation metrics of our method and computed paired Student's *t*-tests on the metrics of the unimodal models previously described. The results of the average evaluation metrics through the 10 folds are shown in Table I.

For the discrimination between CA and AA, our proposed multimodal model outperforms the unimodal ones across all evaluation metrics, with a 2.76% improvement in accuracy over unimodal FC (95.51% vs 92.75%, $p = 0.034$), and a larger increase compared to unimodal SC, which achieved 53.08% ($p = 0.032$). This pattern is consistent across F1-score and precision. Similarly, in the AA vs DA classification, our proposed multimodal model again outperforms both unimodal SC and unimodal FC. The accuracy is 5.04% higher than unimodal FC (93.61% vs 88.57%, $p = 0.016$), and significantly higher than unimodal SC, which achieved 56.48% ($p = 0.016$). This trend is also observed in the F1-score and precision metrics, similar to the CA vs AA discrimination. For CA vs DA, the accuracy of unimodal FC is 7.22% greater than the one in our multimodal model ($p = 0.036$), which is contrary to our expectations. Nevertheless, we notice that the scores with our multimodal approach in this task are still relatively high, about 87%. It is worth noting that our proposed multimodal model achieves the highest scores in two of the three classification tasks across all modalities and almost all metrics (95.51% and 93.61% for accuracies). On the contrary, unimodal SC demonstrates consistently lower performance across all classification tasks, with accuracy ranging from 53.08% to 64.81% and with higher standard deviations. These results suggest that integrating the complex relationship between SC and FC in our multimodal approach induces better classification performance as compared to the unimodal models in most classification tasks. To gain deeper insights into the underlying factors contributing to this, particularly the ROIs driving the discrimination between the groups, we further identify the most salient brain regions in the different models.

TABLE I
CLASSIFICATION PERFORMANCE FOR ALL CLASSIFICATION TASKS ACROSS MODALITIES

	unimodal SC	unimodal FC	Proposed
CA vs AA			
Accuracy	53.08 ± 14.62	92.75 ± 12.79	**95.51 ± 7.90**
F1-score	40.35 ± 16.91	92.82 ± 12.68	**94.84 ± 9.72**
Precision	44.10 ± 26.44	94.72 ± 9.44	**95.44 ± 8.74**
CA vs DA			
Accuracy	64.81 ± 16.09	**93.33 ± 6.24**	86.11 ± 8.78
F1-score	55.43 ± 23.53	**93.43 ± 6.22**	86.37 ± 8.89
Precision	52.22 ± 28.80	**94.59 ± 5.44**	89.07 ± 7.96
AA vs DA			
Accuracy	56.48 ± 17.54	88.57 ± 12.56	**93.61 ± 11.55**
F1-score	42.23 ± 22.21	87.76 ± 14.32	**93.29 ± 12.46**
Precision	34.98 ± 23.96	92.49 ± 7.16	**95.99 ± 6.42**

± represents the standard deviation of evaluation scores through the folds. AA: Anxious Adolescents; CA: Control Adolescents; DA: Depressed Adolescents; FC: Functional Connectivity; SC: Structural Connectivity.

B. Identification of salient ROIs

Fig. 5 shows the averaged localization maps for the top 30 salient ROIs of CA vs AA, CA vs DA, and AA vs DA for the three approaches, computed with Grad-CAM as explained in Section II-D. The names of the top 30 salient ROIs for each classification task are listed in Table 2, Table 3, and Table 4 in the supplemental material.

For CA vs AA, our proposed multimodal approach identified several overlapping ROIs with unimodal FC, including regions from the DMN, such as the prefrontal cortex (PFC)

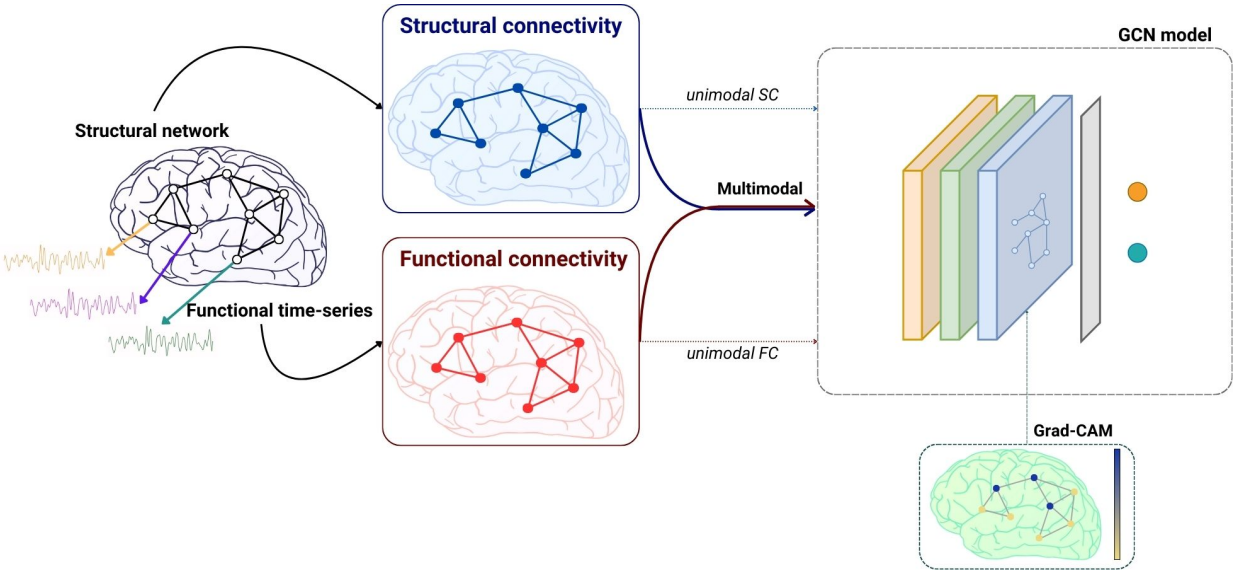

Fig. 4. Experimental pipeline. Structural connectivity is constructed based on diffusion MRI and averaged resting-state fMRI time-series of each brain region (416 regions in total with the Tian-Schaefer atlas) are used to compute functional connectivity, via Pearson correlation coefficient. Then, structural connectivity is used to initialize the graph topology, and functional connectivity is used as the node features. Unimodal approaches with unimodal SC and unimodal FC are developed to enable comparisons with our multimodal approach. Finally, Gradient-weighted Class Activation Mapping is adapted to our graph setting to identify the top brain regions that contribute the most for the classification tasks.

and the dorsal and medial prefrontal cortex (PFCdPFCm). Visual network regions also emerged as key features in both unimodal and multimodal approaches. In particular, 5 ROIs were shared between unimodal FC and our multimodal model, underscoring their importance in driving high classification performance.

For CA vs DA, unimodal FC identifies frontal regions as highly salient, in contrast to the ROIs highlighted in our proposed multimodal model where other networks predominate, such as the visual network, the dorsal attention network (DAN), the somatomotor network (SMN), and also limbic regions with the oribital frontal cortex. Moreover, there is no overlap in the salient ROIs between unimodal FC and our multimodal method. This frontal region involvement and the absence of overlapping ROIs may explain the better performance of unimodal FC in classifying CA vs DA more accurately than our multimodal model.

In the classification of AA vs DA, there is a notable difference in the number of overlapping ROIs between unimodal approaches and our proposed multimodal model. Indeed, 14 ROIs overlap between unimodal SC and our multimodal approach, while this is the case for only one ROI with unimodal FC. The overlapping ROIs between unimodal SC and our multimodal model include key areas within the SMN, visual network, and parts of the DAN. These regions are crucial for distinguishing between AA and DA, contributing to the improved performance observed in our multimodal approach.

For all classification tasks, subcortical regions—namely the hippocampus, putamen, thalamus, and caudate nucleus—are frequently highlighted in unimodal SC and our multimodal model, particularly for CA vs DA. These regions contribute to the model's discriminatory power, especially when combined with cortical regions involved in the DAN and SMN. When considering unimodal methods, several salient ROIs are similar with the ones previously mentioned for our multimodal model. However, most of these ROIs are exclusively identified in one of the unimodal approaches. For example, the subcortical regions are identified in unimodal SC but none appears in unimodal FC. Moreover, the ROIs identified in unimodal FC are mainly part of the DMN, with the PFC, the PFCdPFCm and the precuneus posterior cingulate cortex. Yet, very few of them appear in the top salient ROIs in our proposed multimodal model, but other ROIs are instead highlighted such as the somatomotor cortex and regions from the DAN.

V. Discussion

In this study, we developed a GCN-based framework using graph-structured data combined with node features to classify two groups. This model allows to combine multimodal data, such that the brain graph and feature matrix correspond to SC and the connectivity profile or FC, respectively. It leverages its ability to capture higher-order information from the neighborhoods of graph nodes representing ROI in the SC, while incorporating neural activity from FC.

A. Classification results

Our study achieved an average accuracy of 91.74% in the 3 classification tasks for our multimodal approach, thus demonstrating a competitive classification performance for our multimodal model, with respect to those recently reported using classical machine learning approaches and multi-shell data with the Human Connectome Project protocol [50].

However, the performance of unimodal SC was relatively modest across all 3 classification tasks, suggesting that while SC contributes some structural information, it may not fully

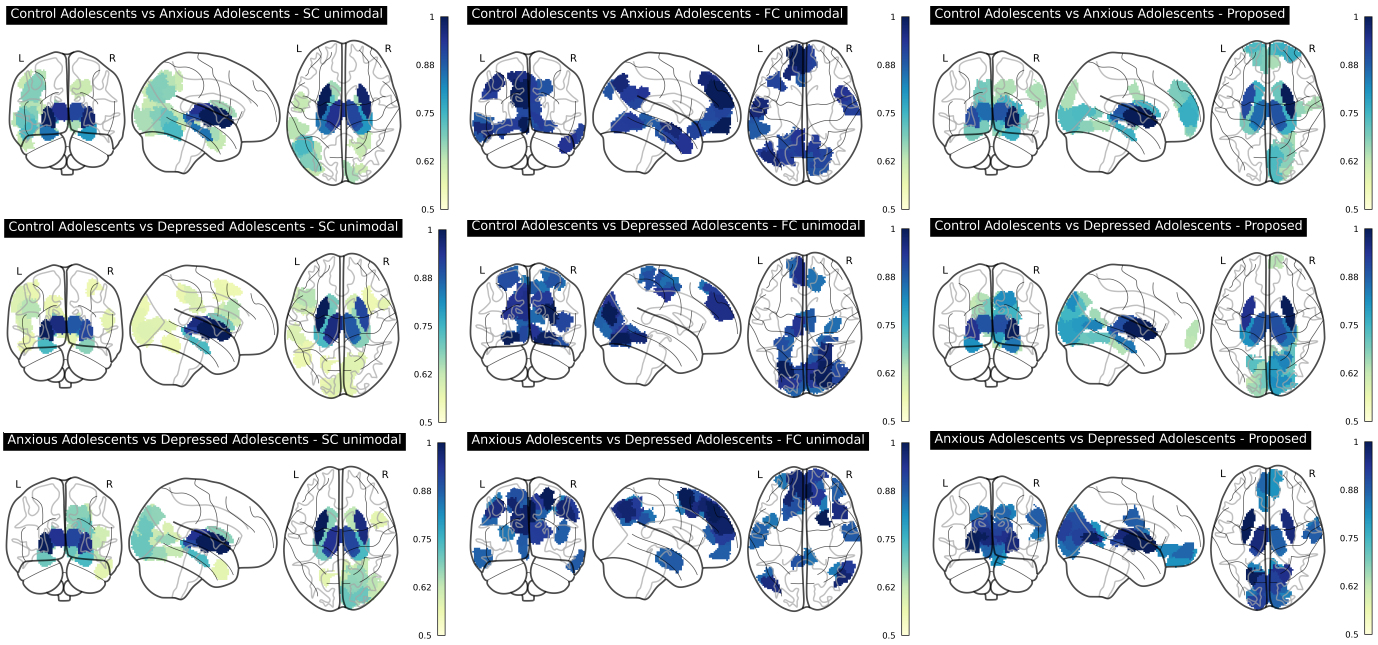

Fig. 5. Localization maps of the 30 regions of interest that discriminate the most between two groups, for all the classification tasks, and across modalities. The fist row corresponds to the classification between Control Adolescents and Anxious Adolescents, the second one between Control Adolescents and Depressed Adolescents, and the third one between Anxious Adolescents and Depressed Adolescents. The first column corresponds to the classification with only structural connectivity information, the second one with only functional connectivity, and the third one with both connectivities. The values on each region were obtained based on Gradient-weighted Class Activation Mapping to reflect the contribution of each of them for the classification task, and were thresholded at 0.5 for visualization purposes such that the values below it were set to 0.

capture the underlying patterns needed for effective classification. This is in agreement with recent reviews that attempted to classify depressed patients from controls, where the best accuracies obtained were less than 60% using DWI [51]–[53]. These results could be attributed to the few structural changes observed in DWI studies in depressed patients [54], [55] and anxious patients [56]. In particular, only subtle alterations were detected in young depressed and anxious populations [57], which may imply that structural brain differences are less pronounced at earlier stages of the disorders, potentially evolving with chronicity or age. Moreover, diffusion models still lack the precision needed to accurately estimate SC, which could further contribute to its limited effectiveness in classification tasks. These models may not fully depict microstructural variations, especially when structural changes are subtle or diffuse across brain regions [58]. Even with the use of more advanced modeling and tracking methods in this work, as presented in Section III, challenges remain, including the reduction of false-positive fibers, the over representation of simpler tracks and the under-representation of difficult ones, leading to a density bias [59]. As such, relying solely on SC may not provide a complete understanding of the complexities involved in distinguishing between the groups.

In contrast, unimodal FC exhibited significantly higher performance, suggesting that FC captures modifications of brain activity that allows to classify the different groups. This highlights the significance of FC in distinguishing connectivity differences relevant to depression and anxiety. Indeed, FC reflects neural activity within networks, which is crucial in psychiatric disorders. Several studies [60], [61] that implemented GCN to classify depressed patients using FC reported classification accuracies around 85%, which is consistent with our results. In comparison to SC, a recent systematic evaluation of machine learning approaches for depression indicated that features derived from fMRI generally outperformed SC in distinguishing depressed patients and controls [51]. This aligns with the idea that FC more closely tracks the brain's real-time communication patterns, whereas SC reflects static pathways, which are less sensitive to transient mental states or disorders like anxiety or depression.

The proposed multimodal approach effectively integrated both SC and FC, allowing us to provide complementary information, where SC defines the physical constraints within which functional activity occurs. This integration enhanced classification performance in specific classification tasks, as evidenced by the results for CA vs AA and AA vs DA. Interestingly, despite the moderate performance of unimodal SC, combining SC with FC yielded higher classification accuracy than using FC alone. This suggests that SC provides a kind of 'structural scaffold' that supports and contextualizes the functional interactions, leading to richer, more nuanced features. For instance, while FC reflects neural activity between brain regions, SC contributes crucial anatomical information that clarifies and strengthens the functional relationships between these regions. This synergy between the two modalities has been demonstrated in prior GCN studies of multimodal brain graphs of SC and FC for classifying neuropsychiatric disorders [62], mild cognitive impairment [63], or autism spectrum disorder [64]. In these works, the inclusion of SC allowed for richer data embeddings from FC, leading to more

accurate clinical predictions. In the classification of CA vs DA, although unimodal FC performed better, our proposed multimodal model achieved high accuracies that were not merely an average of SC and FC performances. On the one hand, this indicates that our model effectively learns the complex relationships between SC and FC, leading to a more nuanced representation of brain connectivity. On the other hand, this may also suggest that DA exhibits more variability in SC patterns, which may hinder the GCN's ability to surpass its performance with AA in the discrimination from CA. This variability in SC might be due to differences in the structural integrity of white matter pathways associated with different groups of depressed patients. Indeed, the literature on depression phenotypes has increasingly highlighted its heterogeneous nature [65], [66], which may influence their SC patterns.

In summary, while SC alone may not provide sufficient information for effective classification, FC offers a robust alternative for clinical data on depression and anxiety. However, the key takeaway is that combining SC and FC in a multimodal approach leverages the complementary strengths of both modalities, resulting in enhanced classification performance that neither modality can achieve alone in specific tasks. This further motivates us to examine the top ROIs that contributed to the discrimination between the groups in our classification tasks, as understanding these key regions may provide deeper insights into the underlying neural mechanisms involved.

B. Altered regions in anxiety and depression

To the best of our knowledge, this is the first investigation using GCN combining structural and functional imaging data to explore the differences between anxious and depressed adolescents. Our study revealed a substantial overlap of networks involved in both conditions (AA and DA) as compared to CA, notably, the DMN that is involved in emotional regulation and self-referential thinking [67]. This network has been commonly identified as associated with these disorders using both structural and functional imaging. It is well known that anxiety and depression share common clinical, and brain components since both are associated with altered affective dimension [68]. Also, it is worth noting that both disorders are highly comorbid, and it is expected that from a pathophysiological standpoint the regions identified with both structural and functional analyses share key networks [69] - such as DMN - involved in emotion regulation [68]. However, anxious and depressed adolescents showed distinct alterations. On the one hand, anxiety seemed to involve more right-lateralized activity in the DMN and changes in visual processing. Although the lateralization of emotion regulation is still debated, some studies have reported that trait anxiety could be associated with the right PFC activation [70]. Consistent with our study, the visual limbic pathway and visual network have been identified to be associated with anxiety state [71] and thought to be involved in abnormal perception of environment visual information [72]. However, the visual network has also been shown to play a role in depressed adolescents in a study using SC-FC coupling [69]. Of note, the salience ventral attentional network (SVAN) has been implicated in AA as compared to CA using multimodal approach but not our depression group. This suggests that disruptions in the SVAN – that has been linked to attention bias - may be more characteristic of anxiety rather than depression, which complements findings from a unimodal rs-fMRI study [73]. Taken together, these abnormalities in the anxious group might be associated with heightened awareness or sensitivity to external stimuli [74]. Our depression group, on the other hand, might be associated with more disruptions in temporal regions of the DMN. These patterns have been linked with rumination and altered emotional memory [75], key aspects of depressive disorder. Even if the DMN – a widely distributed network – seemed to be involved in both depression and anxiety conditions, our study suggested that by combining the two connectivity modalities, some subregions of this network might be more characteristic of depression such as temporal region of the DMN. The multimodal approach might be of interest to have a better precision in exploring some specific pathophysiological patterns related to either anxiety or depressive disorders in adolescents.

C. Differences in salient ROIs between unimodal and multimodal methods

The use of multimodal methods to explore the brain physiology associated with brain development and mental disorders has recently been reported as a promising approach [76]. In our work, our multimodal model tended to highlight more distributed regions within both hemispheres that were related to subcortical structures (like the hippocampus, thalamus, and caudate nucleus), which play key roles in memory, emotion and motivation. These regions are often implicated in depression and anxiety, where structural deficits in regions like the hippocampus correlate with impairments in memory and emotional regulation. For example, studies [77] reported that decreased hippocampal volume is associated with adolescent depression, highlighting the hippocampus's role in the neuropathology of mood disorders. These regions are critical for integrating different neural processes, but might require the sensitivity of multimodal methods to be detected. Unimodal FC highlighted more frequently regions within the DMN, especially in the PFC and parietal cortex. These regions are more involved in higher-order cognitive processes like self-reflection and emotional evaluation, which may exhibit functional changes independent of structural changes. These results suggest that anxiety and depression affect DMN functioning distinctly, which can be captured through FC alone. Unimodal approaches, particularly functional imaging, tend to emphasize activity within DMN regions, often revealing right-hemisphere lateralization in anxiety. This lateralization aligns with evidence that anxiety-related processing engages more right-lateralized brain regions, involved in visual-spatial and threat-related processing [78]. In contrast, structural deficits are more broadly distributed and often encompass areas like the hippocampus and PFC, underlying emotional regulation and memory processes. This distinction in functional and structural changes underscores the utility of multimodal methods to capture a full spectrum of neural alterations across disorders

[79], [80]. These findings collectively suggest that anxiety and depression distinctly alter the DMN and associated networks, with FC alone capable of capturing some disorder-specific patterns. However, combining structural and functional imaging enhances sensitivity, enabling a more nuanced understanding of how these disorders uniquely impact adolescent brain development.

D. Strategies for robust and generalizable models

In this work, we opted for several strategies to enhance classification performance while enabling good generalizability of our multimodal model. We chose the connection profile as the node features for all the modalities. It is believed that such feature encompasses the complete structural information of the brain network, preserving extensive insights on pairwise connections that reflect the full scope of connectivity patterns [81]. Compared to other node features such as fMRI time-series (when FC is considered) or graph topological metrics computed from graph theory, the connection profile has been shown to provide overall higher classification performance in brain connectivity studies applied to clinical data [47]. Other than the choice for the input node features, we also considered multiple techniques to improve generalization of our multimodal model.

GCN, and deep neural networks in general, are highly effective at learning complex relationships between clinical data samples due to their multiple non-linear hidden layers. However, when dealing with few data samples, the model training can lead to overfitting issues. Therefore, a number of strategies have been developed to cope with them. One popular solution is data augmentation, that aims to artificially generate new data based on existing training data [82], [83]. However, this process poses several challenges such as the lack of common evaluation criteria, which sometimes leads to the improvement of the model performance being the only criterion to assess the effectiveness of the augmentation. Another issue arises from the opacity of the models used for data augmentation, making them difficult to interpret [84]. Considering the unknown impacts that augmented SC and FC matrices may have on the interpretation of the salient ROIs, we did not opt for this strategy in our experiments. Instead, we adopted several other techniques and focused on the models' architecture to prevent them from overfitting. First, in our GCN architecture, we included batch normalization [85], a regularization technique that normalizes the activations within a layer by subtracting the batch mean from each activation and dividing by the batch standard deviation. In addition to speeding up the training process, it enhances model stability and generalization. Thus, we applied batch normalization after each GCN layer. Second, we adopted dropout as an additional regularization technique to prevent overfitting. Dropout [86] works by randomly setting a fraction of the neurons to zero during training, forcing the model to rely on different subsets of neurons in each iteration. This technique improves the model's robustness by reducing its dependency on specific neurons and promoting better generalization. In our GCN architecture, dropout was applied after the global average pooling layer and the dense layer with a predefined dropout rate equal to 0.3, ensuring that the model remained resilient and did not overfit to the training data. Third, we implemented early stopping [87], which monitors the model's performance on a validation set during training and halts the process if the validation performance does not improve after a set number of consecutive epochs. This approach helps avoid overtraining, where the model begins to memorize the training data rather than generalizing to unseen data. In our GCN architecture, we applied early stopping with a patience of 20 epochs, ensuring that training stopped at the optimal point to achieve the best generalization.

E. Limitations and future directions

In terms of both performance and interpretation, the present studies yielded strong results given the relatively straightforward structure of our multimodal GCN model. Indeed, the multimodal GCN model and architecture that we considered were relatively simple yet efficient. While effective for integrating SC and FC patterns in a unified framework and extracting the complementary information of both modalities, our proposed multimodal model may not fully exploit the potential of more advanced architectures designed to capture deeper, hierarchical relationships that could be applied to brain networks. With the rapid development of deep learning, GNN followed the trend and several works implemented sophisticated neural network architectures including Long Short-Term Memory [88], graph attention network [89], transformer-based models [90], etc. However, only few works focused on multimodal data in their frameworks, especially in the neuroimaging field applied to neurodegenerative diseases. Investigating these approaches could further allow to leverage the full complexity of SC and FC relationships, potentially enhancing classification performance, though interpretation of the results should be warranted.

Moreover, although the groups of our data were balanced, this study should be replicated in a larger population to assess whether such analysis could provide clearer information on brain changes across the groups and the modalities. Besides, given the findings on our comparative tests with unimodal SC, new tractography methods could enable construction of more robust SC matrices. Studying approaches that add fibers weighting between subcortical and cortical brain regions could be beneficial to reduce the potential over-represented tracks in the subcortical regions.

VI. Conclusion

In this work, we proposed a multimodal multi-layer GCN framework to classify anxious and depressed adolescents with controls by modeling brain spatial and temporal information simultaneously. Despite the large number of previous works that have focused on unimodal approaches with SC and FC to explore the differences between brain connectomes of patients and healthy controls, integrating SC and FC simultaneously in a multimodal GCN model to represent their interactions remains underexplored so far. Using SC as the graph and FC as

the node features, our model effectively combined both modalities and provided high classification performance. In addition, through experimental comparisons with unimodal models, we demonstrated that considering exclusively one modality often output lower classification results, and highlighted salient brain regions that were heavily subject to one only modality as a consequence. In contrast, the joint modeling of SC and FC efficiently exploited the complementary information provided by both modalities, resulting in the identification of brain regions that exhibited significant alterations in patients compared to healthy controls, revealing patterns that aligned more closely with the complexities of brain disorders such as anxiety and depression. We believe that our approach opens the door to a deeper understanding of those diseases, and thus the exploration of new research avenues by clinicians.

ACKNOWLEDGMENT

Data and/or research tools used in the preparation of this manuscript were obtained from the National Institute of Mental Health (NIMH) Data Archive (NDA). NDA is a collaborative informatics system created by the National Institutes of Health to provide a national resource to support and accelerate research in mental health. Dataset identifier(s): 10.15154/3tk5-pb47. This manuscript reflects the views of the authors and may not reflect the opinions or views of the NIH or of the Submitters submitting original data to NDA.

REFERENCES

[1] J. Hohls, H.-H. König, E. Quirke, and A. Hajek, "Anxiety, depression and quality of life—a systematic review of evidence from longitudinal observational studies," *International Journal of Environmental Research and Public Health*, vol. 18, p. 12022, 11 2021.

[2] V. Menon, "Large-scale brain networks and psychopathology: a unifying triple network model," *Trends in Cognitive Sciences*, 2011.

[3] A. Fornito and B. Harrison, "Brain connectivity and mental illness," *Frontiers in Psychiatry*, vol. 3, 2012.

[4] A. Fornito, A. Zalesky, and M. Breakspear, "The connectomics of brain disorders," *Nature reviews. Neuroscience*, vol. 16, pp. 159–72, 02 2015.

[5] B. Jeurissen, M. Descoteaux, S. Mori, and A. Leemans, "Diffusion MRI fiber tractography of the brain," *NMR in Biomedicine*, vol. 32, no. 4, p. e3785, 2019, e3785 NBM-17-0045.R2.

[6] Y. Shi and A. Toga, "Connectome imaging for mapping human brain pathways," *Molecular Psychiatry*, vol. 22, 05 2017.

[7] E. Bullmore and D. Bassett, "Brain graphs: Graphical models of the human brain connectome," *Annual review of clinical psychology*, vol. 7, pp. 113–40, 04 2010.

[8] S. Ayyash, A. Davis, G. Alders, G. MacQueen, S. Strother, S. Hassel, M. Zamyadi, S. Arnott, J. Harris, R. Lam, R. Milev, D. J. Mueller (Müller), S. Kennedy, S. Rotzinger, B. Frey, L. Minuzzi, and G. Hall, "Exploring brain connectivity changes in major depressive disorder using functional-structural data fusion: A CAN-BIND-1 study," *Human Brain Mapping*, vol. 42, 2021.

[9] J.-C. Roy, R. Hedouin, T. Desmidt, S. Dam, I. Mirea-Grivel, W. Louise, E. Bannier, L. Barantin, D. Drapier, J.-M. Batail, R. David, J. Coloigner, and G. Robert, "Quantifying apathy in late-life depression: Unraveling neurobehavioral links through daily activity patterns and brain connectivity analysis," *Biological psychiatry. Cognitive neuroscience and neuroimaging*, vol. 9, 04 2024.

[10] J.-C. Roy, T. Desmidt, S. Dam, I. Mirea-Grivel, L. Weyl, E. Bannier, L. Barantin, D. Drapier, J.-M. Batail, R. David, J. Coloigner, and G. Robert, "Connectivity patterns of the core resting-state networks associated with apathy in late-life depression," *Journal of Psychiatry and Neuroscience*, vol. 48, pp. E404–E413, 2023.

[11] S. Vieira, T. Bolton, M. Schöttner, L. Baecker, A. Marquand, A. Mechelli, and P. Hagmann, "Multivariate brain-behaviour associations in psychiatric disorders," *Translational Psychiatry*, vol. 14, 06 2024.

[12] H. Li, X. Lin, L. Liu, S. Su, X. Zhu, Y. Zheng, W. Huang, J. Que, L. Shi, Y. Bao, L. Lu, J. Deng, and X. Sun, "Disruption of the structural and functional connectivity of the frontoparietal network underlies symptomatic anxiety in late-life depression," *NeuroImage: Clinical*, vol. 28, p. 102398, 2020.

[13] A. Zugman, L. Jett, C. Antonacci, A. M. Winkler, and D. S. Pine, "A systematic review and meta-analysis of resting-state fMRI in anxiety disorders: Need for data sharing to move the field forward," *Journal of Anxiety Disorders*, vol. 99, p. 102773, 2023.

[14] V. Dunn and I. M. Goodyer, "Longitudinal investigation into childhood- and adolescence-onset depression: Psychiatric outcome in early adulthood," *British Journal of Psychiatry*, vol. 188, no. 3, p. 216–222, 2006.

[15] R. Kerestes, C. G. Davey, K. Stephanou, S. Whittle, and B. J. Harrison, "Functional brain imaging studies of youth depression: A systematic review," *NeuroImage: Clinical*, vol. 4, pp. 209–231, 2014.

[16] J. Xu, N. T. Van Dam, C. Feng, Y. Luo, H. Ai, R. Gu, and P. Xu, "Anxious brain networks: A coordinate-based activation likelihood estimation meta-analysis of resting-state functional connectivity studies in anxiety," *Neuroscience & Biobehavioral Reviews*, vol. 96, pp. 21–30, 2019.

[17] J. Zhao, C.-C. Huang, Y. Zhang, Y. Liu, S.-J. Tsai, and C.-Y. Lo, "Structure-function coupling in white matter uncovers the abnormal brain connectivity in schizophrenia," *Translational psychiatry*, 2023.

[18] X. Xu, S. Xu, L. Han, and X. Yao, "Coupling analysis between functional and structural brain networks in Alzheimer's disease," *Mathematical Biosciences and Engineering*, 2022.

[19] L. E. Suárez, R. D. Markello, R. F. Betzel, and B. Misic, "Linking structure and function in macroscale brain networks," *Trends in Cognitive Sciences*, vol. 24, no. 4, pp. 302–315, 2020.

[20] S. Liu, W. Cai, S. Liu, F. Zhang, M. Fulham, D. D. F. Feng, S. Pujol, and R. Kikinis, "Multimodal neuroimaging computing: A review of the applications in neuropsychiatric disorders," *Brain Informatics*, vol. 2, pp. 167–180, 08 2015.

[21] J. Yang, Y. Yin, Z. Zhang, J. Long, J. Dong, Y. Zhang, Z. Xu, L. Li, J. Liu, and Y. Yuan, "Predictive brain networks for major depression in a semi-multimodal fusion hierarchical feature reduction framework," *Neuroscience Letters*, vol. 665, pp. 163–169, 2018.

[22] J. Sui, D. Zhi, and V. Calhoun, "Data-driven multimodal fusion: approaches and applications in psychiatric research," *Psychoradiology*, vol. 3, 11 2023.

[23] L. A. Maglanoc, T. Kaufmann, R. Jonassen, E. Hilland, D. Beck, N. I. Landrø, and L. T. Westlye, "Multimodal fusion of structural and functional brain imaging in depression using linked independent component analysis," *Human Brain Mapping*, vol. 41, no. 1, pp. 241–255, 2020.

[24] E. Damaraju, R. F. Silva, T. Adali, and V. D. Calhoun, "A multimodal IVA fusion approach to identify linked neuroimaging markers," in *2021 43rd Annual International Conference of the IEEE Engineering in Medicine & Biology Society (EMBC)*, 2021, pp. 3928–3932.

[25] G. Leus, A. G. Marques, J. M. Moura, A. Ortega, and D. I. Shuman, "Graph signal processing: History, development, impact, and outlook," *IEEE Signal Processing Magazine*, vol. 40, no. 4, pp. 49–60, 2023.

[26] P. J. Thomas, A. Leow, H. Klumpp, K. L. Phan, and O. Ajilore, "Default mode network hypoalignment of function to structure correlates with depression and rumination," *Biological Psychiatry: Cognitive Neuroscience and Neuroimaging*, vol. 9, no. 1, pp. 101–111, 2024.

[27] S. Dam, P. Maurel, and J. Coloigner, "Graph Wavelet Packets for the Classification of Brain Data in Anxiety and Depression," in *EUSIPCO 2024 - 32nd European conference on signal processing*, Lyon, France, Aug. 2024.

[28] H. Padole, S. Joshi, and T. K. Gandhi, "Early detection of Alzheimer's disease using graph signal processing on neuroimaging data," in *2018 2nd European Conference on Electrical Engineering and Computer Science (EECS)*, 2018, pp. 302–306.

[29] T. N. Kipf and M. Welling, "Semi-supervised classification with graph convolutional networks," in *5th International Conference on Learning Representations, ICLR 2017*, 2017.

[30] Y. Li, Y. Zou, H. Guo, Y. Yang, N. Li, L. Li, and F. Zhao, "Identification of Mild cognitive impairment based on quadruple GCN model constructed with multiple features from higher-order brain connectivity," *Expert Systems with Applications*, vol. 230, p. 120575, 2023.

[31] L. Wang, K. Li, and X. P. Hu, "Graph convolutional network for fMRI analysis based on connectivity neighborhood," *Network Neuroscience*, vol. 5, no. 1, pp. 83–95, 02 2021.

[32] S. I. Ktena, S. Parisot, E. Ferrante, M. Rajchl, M. Lee, B. Glocker, and D. Rueckert, "Metric learning with spectral graph convolutions on brain connectivity networks," *NeuroImage*, vol. 169, pp. 431–442, 2018.

[33] X. Zhao, J. Wu, H. Peng, A. Beheshti, J. J. Monaghan, D. McAlpine, H. Hernandez-Perez, M. Dras, Q. Dai, Y. Li, P. S. Yu, and L. He, "Deep reinforcement learning guided graph neural networks for brain network analysis," *Neural Networks*, vol. 154, pp. 56–67, 2022.

[34] L. Zhang, A. Zaman, L. Wang, J. Yan, and D. Zhu, "A cascaded multi-modality analysis in mild cognitive impairment," in *Machine Learning in Medical Imaging*. Springer International Publishing, 2019, pp. 557–565.

[35] R. R. Selvaraju, M. Cogswell, A. Das, R. Vedantam, D. Parikh, and D. Batra, "Grad-CAM: Visual explanations from deep networks via gradient-based localization." in *ICCV*. IEEE Computer Society, 2017, pp. 618–626.

[36] V. Siless, N. A. Hubbard, R. Jones, J. Wang, N. Lo, C. C. Bauer, M. Goncalves, I. Frosch, D. Norton, G. Vergara, K. Conroy, F. V. De Souza, I. M. Rosso, A. H. Wickham, E. A. Cosby, M. Pinaire, D. Hirshfeld-Becker, D. A. Pizzagalli, A. Henin, S. G. Hofmann, R. P. Auerbach, S. Ghosh, J. Gabrieli, S. Whitfield-Gabrieli, and A. Yendiki, "Image acquisition and quality assurance in the boston adolescent neuroimaging of depression and anxiety study," *NeuroImage: Clinical*, vol. 26, p. 102242, 2020.

[37] M. Defferrard, X. Bresson, and P. Vandergheynst, "Convolutional neural networks on graphs with fast localized spectral filtering," in *Advances in Neural Information Processing Systems*, D. Lee, M. Sugiyama, U. Luxburg, I. Guyon, and R. Garnett, Eds., vol. 29. Curran Associates, Inc., 2016.

[38] V. Jahmunah, E. Ng, R.-S. Tan, S. L. Oh, and U. R. Acharya, "Explainable detection of myocardial infarction using deep learning models with Grad-CAM technique on ECG signals," *Computers in Biology and Medicine*, vol. 146, p. 105550, 2022.

[39] H. Panwar, P. Gupta, M. K. Siddiqui, R. Morales-Menendez, P. Bhardwaj, and V. Singh, "A deep learning and grad-CAM based color visualization approach for fast detection of COVID-19 cases using chest X-ray and CT-Scan images," *Chaos, Solitons & Fractals*, vol. 140, p. 110190, 2020.

[40] M. Cieslak, P. Cook, X.-S. He, F.-C. Yeh, T. Dhollander, A. Adebimpe, G. Aguirre, D. Bassett, R. Betzel, J. Bourque, L. Cabral, C. Davatzikos, J. Detre, E. Earl, M. Elliott, S. Fadnavis, D. Fair, W. Foran, P. Fotiadis, and T. Satterthwaite, "QSIPrep: an integrative platform for preprocessing and reconstructing diffusion MRI data," *Nature Methods*, 2021.

[41] O. Esteban, C. J. Markiewicz, R. W. Blair, C. A. S. Moodie, A. I. Isik, A. Erramuzpe, J. D. Kent, M. Goncalves, E. Dupre, M. Snyder, H. Oya, S. S. Ghosh, J. Wright, J. Durnez, R. A. Poldrack, and K. J. Gorgolewski, "fMRIPrep: a robust preprocessing pipeline for functional mri," *Nature methods*, vol. 16, pp. 111 – 116, 2018.

[42] J. Veraart, E. Fieremans, and D. S. Novikov, "Diffusion MRI noise mapping using random matrix theory," *Magnetic Resonance in Medicine*, vol. 76, no. 5, pp. 1582–1593, 2016.

[43] M. Jenkinson, C. F. Beckmann, T. E. Behrens, M. W. Woolrich, and S. M. Smith, "FSL," *NeuroImage*, vol. 62, no. 2, pp. 782–790, 2012.

[44] A. Schaefer, R. Kong, E. M. Gordon, T. O. Laumann, X.-N. Zuo, A. J. Holmes, S. B. Eickhoff, and B. T. T. Yeo, "Local-Global Parcellation of the Human Cerebral Cortex from Intrinsic Functional Connectivity MRI," *Cerebral Cortex*, vol. 28, no. 9, pp. 3095–3114, 2017.

[45] Y. Tian, D. S. Margulies, M. Breakspear, and A. Zalesky, "Topographic organization of the human subcortex unveiled with functional connectivity gradients," *Nature Neuroscience*, 2020.

[46] R. E. Smith, J.-D. Tournier, F. Calamante, and A. Connelly, "SIFT2: Enabling dense quantitative assessment of brain white matter connectivity using streamlines tractography," *NeuroImage*, vol. 119, pp. 338–351, 2015.

[47] G. Wang, L. Zhang, and L. Qiao, "The effect of node features on GCN-based brain network classification: an empirical study," *PeerJ*, vol. 11, p. e14835, Mar. 2023.

[48] X. Glorot and Y. Bengio, "Understanding the difficulty of training deep feedforward neural networks," in *Proceedings of the Thirteenth International Conference on Artificial Intelligence and Statistics*, ser. Proceedings of Machine Learning Research, Y. W. Teh and M. Titterington, Eds., vol. 9. Chia Laguna Resort, Sardinia, Italy: PMLR, 13–15 May 2010, pp. 249–256.

[49] M. Fey and J. E. Lenssen, "Fast graph representation learning with PyTorch Geometric," in *ICLR Workshop on Representation Learning on Graphs and Manifolds*, 2019.

[50] J. Anbarasi, R. Kumari, M. Ganesh, and R. Agrawal, "Translational connectomics: overview of machine learning in macroscale connectomics for clinical insights," *BMC Neurology*, vol. 24, 09 2024.

[51] N. R. Winter, J. Blanke, R. Leenings, J. Ernsting, L. Fisch, K. Sarink, C. Barkhau, D. Emden, K. Thiel, K. Flinkenflügel, A. Winter, J. Goltermann, S. Meinert, K. Dohm, J. Repple, M. Gruber, E. J. Leehr, N. Opel, D. Grotegerd, R. Redlich, R. Nitsch, J. Bauer, W. Heindel, J. Gross, B. Risse, T. F. M. Andlauer, A. J. Forstner, M. M. Nöthen, M. Rietschel, S. G. Hofmann, J.-K. Pfarr, L. Teutenberg, P. Usemann, F. Thomas-Odenthal, A. Wroblewski, K. Brosch, F. Stein, A. Jansen, H. Jamalabadi, N. Alexander, B. Straube, I. Nenadić, T. Kircher, U. Dannlowski, and T. Hahn, "A Systematic Evaluation of Machine Learning–Based Biomarkers for Major Depressive Disorder," *JAMA Psychiatry*, vol. 81, no. 4, pp. 386–395, 04 2024.

[52] A. Stolicyn, M. Harris, X. Shen, M. Barbu, M. Adams, E. Hawkins, L. de Nooij, H. W. Yeung, A. Murray, S. Lawrie, J. Steele, A. Mcintosh, and H. Whalley, "Automated classification of depression from structural brain measures across two independent community-based cohorts," *Human Brain Mapping*, vol. 41, 06 2020.

[53] Z. Gracia-Tabuenca, E. B. Barbeau, Y. Xia, and X. Chai, "Predicting depression risk in early adolescence via multimodal brain imaging," *NeuroImage: Clinical*, vol. 42, p. 103604, 2024.

[54] C. Lynch, I. Elbau, T. Ng, A. Ayaz, S. Zhu, D. Wolk, N. Manfredi, M. Johnson, M. Chang, J. Chou, I. Summerville, C. Ho, M. Lückel, H. Bukhari, D. Buchanan, L. Victoria, N. Solomonov, E. Goldwaser, S. Moia, and C. Liston, "Frontostriatal salience network expansion in individuals in depression," *Nature*, vol. 633, pp. 624–633, 09 2024.

[55] N. R. Winter, R. Leenings, J. Ernsting, K. Sarink, L. Fisch, D. Emden, J. Blanke, J. Goltermann, N. Opel, C. Barkhau, S. Meinert, K. Dohm, J. Repple, M. Mauritz, M. Gruber, E. J. Leehr, D. Grotegerd, R. Redlich, A. Jansen, I. Nenadic, M. M. Nöthen, A. Forstner, M. Rietschel, J. Groß, J. Bauer, W. Heindel, T. Andlauer, S. B. Eickhoff, T. Kircher, U. Dannlowski, and T. Hahn, "Quantifying Deviations of Brain Structure and Function in Major Depressive Disorder Across Neuroimaging Modalities," *JAMA Psychiatry*, vol. 79, no. 9, pp. 879–888, 09 2022.

[56] C. Yang, Y. Zhang, M. Lu, J. Ren, and Z. Li, "White matter structural brain connectivity of young healthy individuals with high trait anxiety," *Frontiers in Neurology*, vol. 10, 2020.

[57] Y. Hung, Z. M. Saygin, J. Biederman, D. Hirshfeld-Becker, M. Uchida, O. Doehrmann, M. Han, X. J. Chai, T. Kenworthy, P. Yarmak, S. L. Gaillard, S. Whitfield-Gabrieli, and J. D. E. Gabrieli, "Impaired Frontal-Limbic White Matter Maturation in Children at Risk for Major Depression," *Cerebral Cortex*, vol. 27, no. 9, pp. 4478–4491, 09 2016.

[58] N. A. Seider, B. Adeyemo, R. Miller, D. J. Newbold, J. M. Hampton, K. M. Scheidter, J. Rutlin, T. O. Laumann, J. L. Roland, D. F. Montez, A. N. Van, A. Zheng, S. Marek, B. P. Kay, G. L. Bretthorst, B. L. Schlaggar, D. J. Greene, Y. Wang, S. E. Petersen, D. M. Barch, E. M. Gordon, A. Z. Snyder, J. S. Shimony, and N. U. Dosenbach, "Accuracy and reliability of diffusion imaging models," *NeuroImage*, vol. 254, p. 119138, 2022.

[59] K. Maier-Hein, P. Neher, J.-C. Houde, M.-A. Côté, E. Garyfallidis, J. Zhong, M. Chamberland, F.-C. Yeh, Y.-C. Lin, Q. Ji, W. Reddick, J. Glass, D. Chen, F. Yuanjing, C. Gao, Y. Wu, J. Ma, H. Renjie, Q. Li, and M. Descoteaux, "The challenge of mapping the human connectome based on diffusion tractography," *Nature Communications*, vol. 8, 11 2017.

[60] Y. Kong, S. Gao, Y. Yue, Z. Hou, H. Shu, C. Xie, Z. Zhang, and Y. Yuan, "Spatio-temporal graph convolutional network for diagnosis and treatment response prediction of major depressive disorder from functional connectivity," *Human Brain Mapping*, vol. 42, no. 12, pp. 3922–3933, 2021.

[61] K. Qin, D. Lei, W. H. Pinaya, N. Pan, W. Li, Z. Zhu, J. A. Sweeney, A. Mechelli, and Q. Gong, "Using graph convolutional network to characterize individuals with major depressive disorder across multiple imaging sites," *eBioMedicine*, vol. 78, p. 103977, 2022.

[62] L. Liu, Y.-P. Wang, Y. Wang, P. Zhang, and S. Xiong, "An enhanced multi-modal brain graph network for classifying neuropsychiatric disorders," *Medical Image Analysis*, vol. 81, p. 102550, 2022.

[63] L. Zhang, L. Wang, J. Gao, S. L. Risacher, J. Yan, G. Li, T. Liu, and D. Zhu, "Deep fusion of brain structure-function in mild cognitive impairment," *Medical Image Analysis*, vol. 72, p. 102082, 2021.

[64] N. S. Dsouza, M. B. Nebel, D. Crocetti, J. Robinson, S. Mostofsky, and A. Venkataraman, "M-GCN: A multimodal graph convolutional network to integrate functional and structural connectomics data to predict multidimensional phenotypic characterizations," in *Proceedings of the Fourth Conference on Medical Imaging with Deep Learning*, ser. Proceedings of Machine Learning Research, M. Heinrich, Q. Dou, M. de Bruijne, J. Lellmann, A. Schläfer, and F. Ernst, Eds., vol. 143. PMLR, 07–09 Jul 2021, pp. 119–130.

[65] B. Jermy, K. Glanville, J. Coleman, C. Lewis, and E. Vassos, "Exploring the genetic heterogeneity in major depression across diagnostic criteria," *Molecular Psychiatry*, vol. 26, no. 12, Jul. 2021.

[66] A. N. Goldstein-Piekarski, T. M. Ball, Z. Samara, B. R. Staveland, A. S. Keller, S. L. Fleming, K. A. Grisanzio, B. Holt-Gosselin, P. Stetz, J. Ma, and L. M. Williams, "Mapping neural circuit biotypes to symptoms and behavioral dimensions of depression and anxiety," *Biological Psychiatry*, vol. 91, no. 6, pp. 561–571, 2022, predicting the Natural History and Treatment Response in Mood Disorders.

[67] Y. I. Sheline, D. M. Barch, J. L. Price, M. M. Rundle, S. N. Vaishnavi, A. Z. Snyder, M. A. Mintun, S. Wang, R. S. Coalson, and M. E. Raichle, "The default mode network and self-referential processes in depression," *Proceedings of the National Academy of Sciences*, vol. 106, no. 6, pp. 1942–1947, 2009.

[68] E. T. Dobson, P. E. Croarkin, H. K. Schroeder, S. T. Varney, S. A. Mossman, K. Cecil, and J. R. Strawn, "Bridging anxiety and depression: A network approach in anxious adolescents," *Journal of Affective Disorders*, vol. 280, pp. 305–314, 2021.

[69] M. Xu, X. Li, T. Teng, Y. Huang, M. Liu, Y. Long, F. Lv, D. Zhi, X. Li, A. Feng, S. Yu, V. Calhoun, X. Zhou, and J. Sui, "Reconfiguration of Structural and Functional Connectivity Coupling in Patient Subgroups With Adolescent Depression," *JAMA Network Open*, vol. 7, no. 3, pp. e241 933–e241 933, 03 2024.

[70] E. H. Telzer, K. Mogg, B. P. Bradley, X. Mai, M. Ernst, D. S. Pine, and C. S. Monk, "Relationship between trait anxiety, prefrontal cortex, and attention bias to angry faces in children and adolescents," *Biological Psychology*, vol. 79, no. 2, pp. 216–222, 2008.

[71] M. Liao, F. Yang, Y. Zhang, Z. He, L. Su, and L. Li, "White matter abnormalities in adolescents with generalized anxiety disorder: A diffusion tensor imaging study," *BMC psychiatry*, vol. 14, p. 41, 02 2014.

[72] J. Choi, B. Jeong, A. Polcari, M. L. Rohan, and M. H. Teicher, "Reduced fractional anisotropy in the visual limbic pathway of young adults witnessing domestic violence in childhood," *NeuroImage*, vol. 59, no. 2, pp. 1071–1079, 2012.

[73] C. M. Sylvester, D. M. Barch, M. Corbetta, J. D. Power, B. L. Schlaggar, and J. L. Luby, "Resting state functional connectivity of the ventral attention network in children with a history of depression or anxiety," *Journal of the American Academy of Child & Adolescent Psychiatry*, vol. 52, no. 12, pp. 1326–1336.e5, 2013.

[74] Q. Ding, J. Xu, S. Peng, J. Chen, Y. Luo, X. Li, R. Wu, X. Li, and S. Qin, "Brain network integration underpins differential susceptibility of adolescent anxiety," *Psychological Medicine*, vol. 54, no. 1, p. 193–202, 2024.

[75] D. Willinger, I. Häberling, I. Ilioska, G. Berger, S. Walitza, and S. Brem, "Weakened effective connectivity between salience network and default mode network during resting state in adolescent depression," *Frontiers in Psychiatry*, vol. 15, 2024.

[76] Y. Jiang, Y. Mu, Z. Xu, Q. Liu, S. Wang, H. Wang, and J. Feng, "Identifying individual brain development using multimodality brain network," *Communications Biology*, vol. 7, 09 2024.

[77] F. P. MacMaster, Y. Mirza, P. R. Szeszko, L. E. Kmiecik, P. C. Easter, S. P. Taormina, M. Lynch, M. Rose, G. J. Moore, and D. R. Rosenberg, "Amygdala and hippocampal volumes in familial early onset major depressive disorder," *Biological Psychiatry*, vol. 63, no. 4, pp. 385–390, 2008, stress, Depression, and Circuitry.

[78] E. Silberman and H. J. Weingartner, "Hemispheric lateralization of functions related to emotion," *Brain and Cognition*, vol. 5, pp. 322–353, 1986.

[79] C. Yang, Z. Zhou, W. Bao, R. Zhong, M. Tang, Y. Wang, Y. Gao, X. Hu, L. Zhang, L. Qiu, W. Kuang, X. Huang, and Q. Gong, "Sex differences in aberrant functional connectivity of three core networks and subcortical networks in medication-free adolescent-onset major depressive disorder," *Cerebral Cortex*, vol. 34, no. 6, p. bhae225, 06 2024.

[80] S. Xie, X. Zhang, W. Cheng, and Z. Yang, "Adolescent anxiety disorders and the developing brain: Comparing neuroimaging findings in adolescents and adults," *General Psychiatry*, vol. 34, p. e100411, 08 2021.

[81] H. Cui, W. Dai, Y. Zhu, X. Kan, A. A. C. Gu, J. Lukemire, L. Zhan, L. He, Y. Guo, and C. Yang, "BrainGB: A benchmark for brain network analysis with graph neural networks," *IEEE Transactions on Medical Imaging*, vol. 42, pp. 493–506, 2022.

[82] B. Barile, A. Marzullo, C. Stamile, F. Durand-Dubief, and D. Sappey-Marinier, "Data augmentation using generative adversarial neural networks on brain structural connectivity in multiple sclerosis," *Computer Methods and Programs in Biomedicine*, vol. 206, p. 106113, 2021.

[83] C. Li, Y. Wei, X. Chen, and C.-B. Schönlieb, "BrainNetGAN: Data augmentation of brain connectivity using generative adversarial network for dementia classification," in *Deep Generative Models, and Data Augmentation, Labelling, and Imperfections*, S. Engelhardt, I. Oksuz, D. Zhu, Y. Yuan, A. Mukhopadhyay, N. Heller, S. X. Huang, H. Nguyen, R. Sznitman, and Y. Xue, Eds. Cham: Springer International Publishing, 2021, pp. 103–111.

[84] T. Islam, M. S. Hafiz, J. R. Jim, M. M. Kabir, and M. Mridha, "A systematic review of deep learning data augmentation in medical imaging: Recent advances and future research directions," *Healthcare Analytics*, vol. 5, p. 100340, 2024.

[85] S. Ioffe, "Batch normalization: Accelerating deep network training by reducing internal covariate shift," *arXiv preprint arXiv:1502.03167*, 2015.

[86] N. Srivastava, G. Hinton, A. Krizhevsky, I. Sutskever, and R. Salakhutdinov, "Dropout: A simple way to prevent neural networks from overfitting," *Journal of Machine Learning Research*, vol. 15, no. 56, pp. 1929–1958, 2014.

[87] R. Caruana, S. Lawrence, and C. Giles, "Overfitting in neural nets: Backpropagation, conjugate gradient, and early stopping," 2001.

[88] L. Liu, G. Wen, P. Cao, T. Hong, J. Yang, X. Zhang, and O. R. Zaiane, "BrainTGL: A dynamic graph representation learning model for brain network analysis," *Computers in Biology and Medicine*, vol. 153, p. 106521, 2023.

[89] C. Dong and D. Sun, "Brain network classification based on dynamic graph attention information bottleneck," *Computer Methods and Programs in Biomedicine*, vol. 243, p. 107913, 2024.

[90] X. Kan, W. Dai, H. Cui, Z. Zhang, Y. Guo, and C. Yang, "Brain network transformer," in *Advances in Neural Information Processing Systems*, 2022.